Supplemental Figures

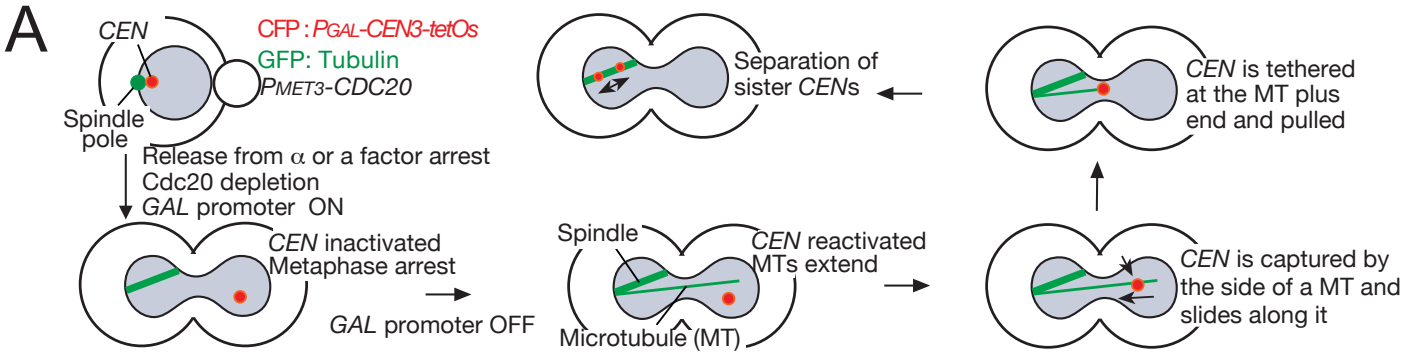

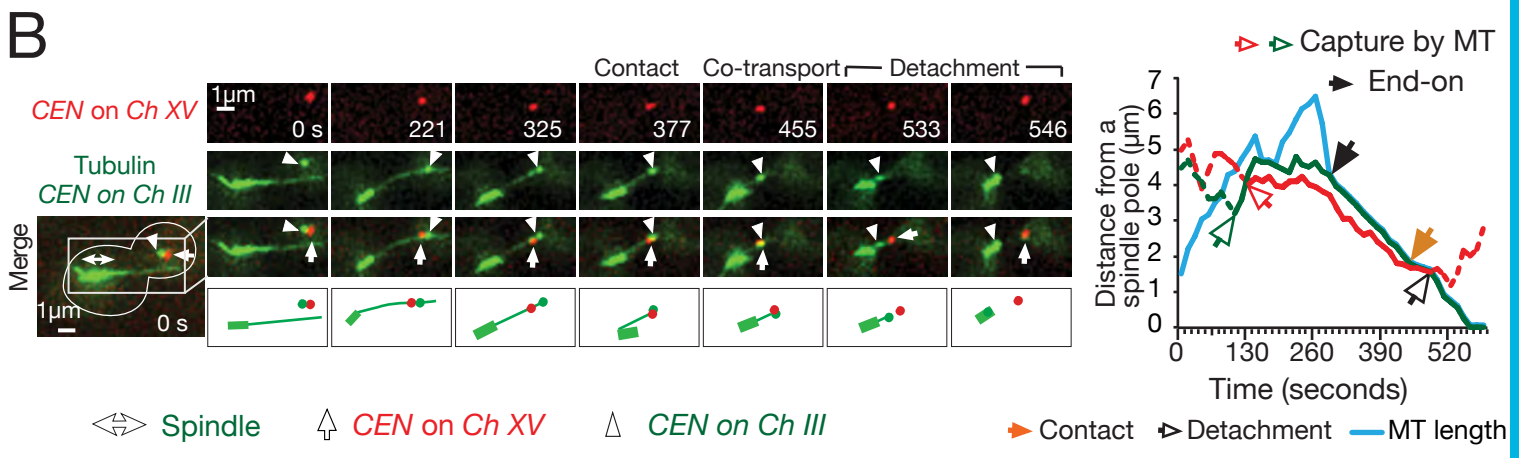

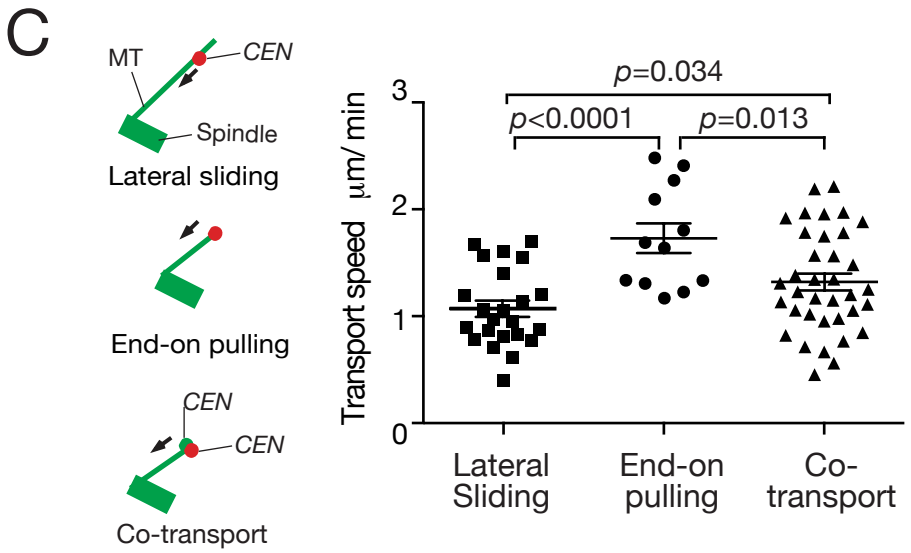

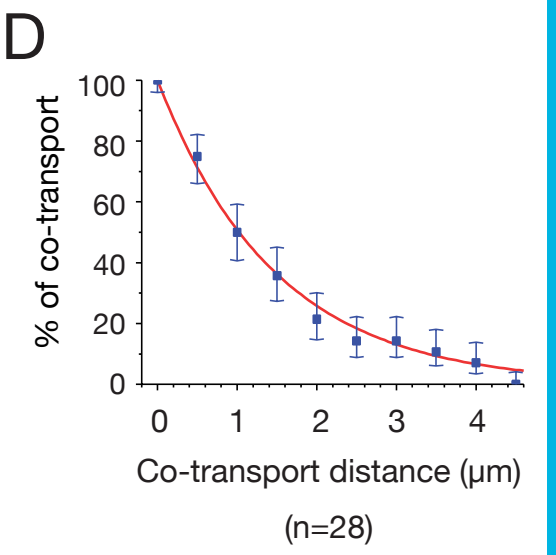

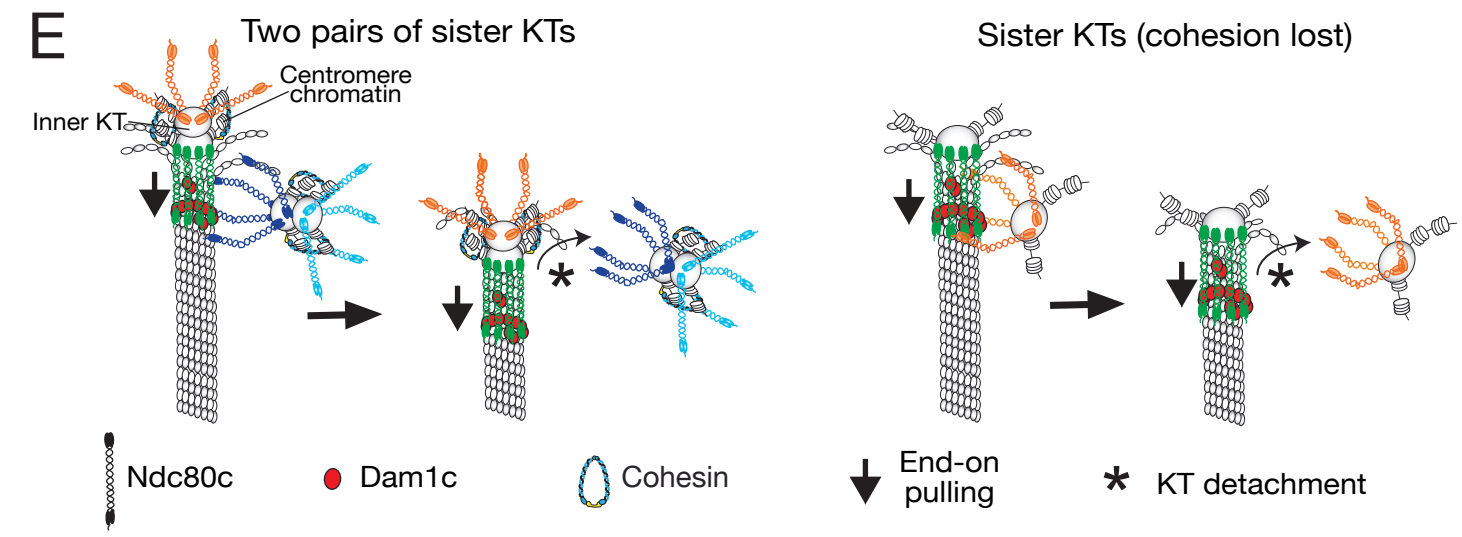

Figure S1. Supplemental Figure associated with Figures 1 and 2

A) Engineered assay system to analyze individual KT–MT interactions with high spatial resolution in budding yeast (Tanaka et al., 2005). CFP: cyan fluorescent protein. GFP: green fluorescent protein.

B) Another representative example (in addition to Figure 1D) where an originally laterally attached KT showed detachment from the MT end after coming into contact with an end-on attached KT. T9717 cells (see Figure 1D) were treated as in Figure 1C. Images and graphs are shown as in Figure 1C. Note that the weak green signal at *CEN* on chromosome XV at 325 s and 546 s likely comes from KT-associated MTs (Kitamura et al., 2010).

C) Diagram on left shows three KT transport modes (lateral sliding, end-on pulling and co-transport). Graph on right shows KT transport speed with the three transport modes. T9717 cells (see Figure 1D) were treated as in Figure 1C. In each mode of transport, the transport speed of P_{GAL}-*CEN3* on chromosome XV (*tetO* fluorescent dot) was measured. Graphs show individual data points and mean ± SEM. The speed of the lateral sliding along a MT was evaluated when *CEN* moved continuously for 1 μm or more in one direction. The sliding speed of P_{GAL}-*CEN3* on chromosome XV was very similar in the presence and absence of P_{GAL}-*CEN3* on chromosome III (*lacO* fluorescent dot) on the lateral side of the same MT.

D) Detachment of *CEN* from the MT end occurs at an approximately constant rate during co-transports of two *CEN*s following their contact (refer to the diagram in Figure 1B). The images collected for Figure 1D were analyzed further. The graph shows how the percentage of co-transports of *CEN*s decreases as the co-transport proceeds and detachment of one *CEN* takes place. The data points in blue show the measured percentage, the error bars represent standard errors of proportions, and a red line shows a regression curve (a simple exponential decay curve). The percentage of remaining co-transports (in which detachment of one *CEN* has not occurred yet) declines approximately following a simple exponential decay curve. This suggests that detachment of one *CEN* happens approximately at a constant rate (per length of a co-transport).

E) Diagrams show models about how an end-on attached KT excludes a laterally attached KT from forming the end-on attachment and causes its detachment from the MT. On the left, two pairs of sister KTs are on one MT. One forms the end-on attachment, while the other interacts with the MT lateral side, close to the MT end, and subsequently detaches from the MT. We speculate that, while one sister KT attaches to the MT end, the other sister is not involved in MT attachment, since one sister KT is sufficient to form 'exclusive' end on attachment (see right; Figure 2). On the right, two sister KTs, which are separate from each other due to a loss of cohesion, interact with one MT. One sister forms the end-on attachment, while the other sister interacts with the MT lateral side (close to the MT end) and subsequently detaches from the MT. The Ndc80 and Dam1 complexes of KTs interact with each other to configure end-on attachment, (Gonen et al., 2012; Kalantzaki et al., 2015; Lampert et al., 2010; Maure et al., 2011; Tien et al., 2010) while the Ndc80, but not the Dam1 complex, are involved in lateral KT–MT interaction (Kalantzaki et al., 2015; Tanaka et al., 2007). The diagrams show speculative configuration of these complexes. The Ndc80 complexes on each sister KT are highlighted in different colors.

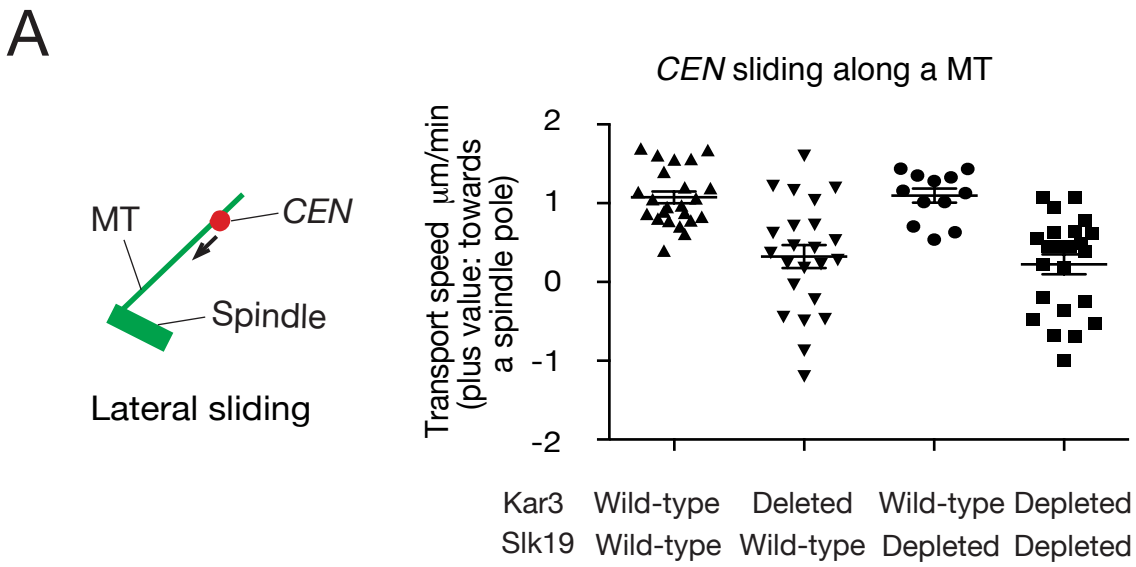

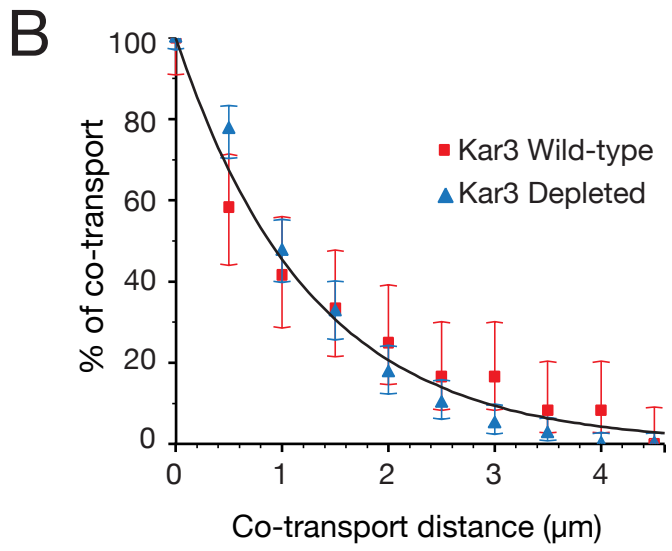

Figure S2. Supplemental Figure associated with Figure 3

A) Kar3 promotes KT sliding along a MT, similarly in the presence and absence of Slk19. To address the effects of KT sliding along a MT on the positions and frequency of KT detachments, we needed to analyze KT behavior in several samples in the presence and absence of Kar3, where two *CEN*s (two pairs of sister *CEN*s), not associated with each other, were caught separately on the MT lateral side. However, contrary to our requirements, two *CEN*s were often associated with each other, prior to the MT interaction after metaphase arrest. Such association was observed after cells were arrested in mitosis (e.g. with nocodazole (Richmond et al., 2013) or Cdc20 depletion), but not observed in physiological conditions. Association between multiple *CEN*s is dependent on Slk19 when cells are arrested in mitosis (Richmond et al., 2013). Therefore, to ensure the two reactivated *CEN*s separate from each other, we depleted Slk19 and compared the behaviors of *CEN*s in Kar3 wild type and Kar3-depleted (or *kar3*Δ) cells. *KAR3*+ (T9717) and *kar3*Δ (T10013) cells with *SLK19*+ P_{GAL}-*CEN3-tetOs* (replacing *CEN15*) *TetR-3×CFP* P_{GAL}-*CEN3-lacO* (replacing *CEN3*) *GFP-LacI GFP-TUB1* P_{MET3}-*CDC20* were treated as in Figure 1C, and images (CFP and GFP signals) were acquired every 13 sec. Meanwhile, *KAR3*+ (T11497) and *kar3-aid* (T11469) cells with *slk19-mini-aid TIR1* P_{GAL}-*CEN3-tetOs* (replacing *CEN15*) *TetR-3×CFP* P_{GAL}-*CEN3-lacO* (replacing *CEN3*) *GFP-LacI-GFP GFP-TUB1* P_{MET3}-*CDC20* were treated as in Figure 3A, and images (CFP and GFP signals) were acquired every 18 sec. The speed of the *CEN3-tetOs* motion along a MT was evaluated i) when it moved continuously for 1 μm or more in one direction, or ii) when it was present on a MT lateral side (without reaching a spindle or being converted to end-on attachment) for 1 min or longer. Graphs show individual data points and mean ± SEM. The results suggest that Kar3 facilitates KT sliding along a MT towards a spindle pole, to a similar extent with and without Slk19.

B) Detachment of *CEN* from the MT end occurs at a similar rate in Kar3 wild-type and Kar3-depleted cells, during co-transports of two *CEN*s following their contact (refer to the diagram in Figure 1B). The images collected for Figure 3 were analyzed further. The graph shows how the percentage of co-transports of *CEN*s decreases as the co-transport proceeds and detachment of one *CEN* takes place. The measured percentage is shown for Kar3 wild-type (red squares) and Kar3-depleted (blue triangles) cells and the error bars represent standard errors of proportions. The percentage of remaining co-transports (in which detachment of one *CEN* has not occurred yet) declines similarly between Kar3 wild-type and Kar3-depleted cells, suggesting that the rate of *CEN* detachment (per length of a co-transport) is similar between the two cells. The percentage also declines approximately following a simple exponential decay curve (black line), suggesting that detachment of one *CEN* happens approximately at a constant rate.

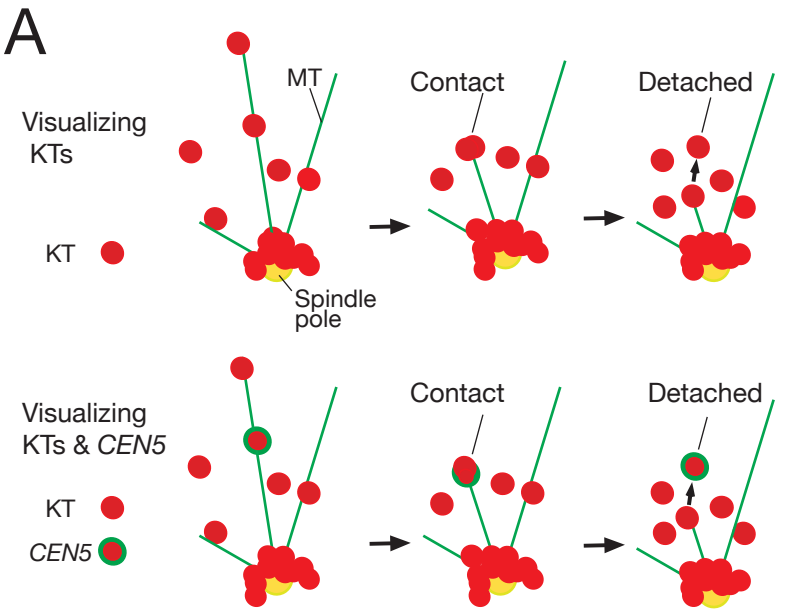

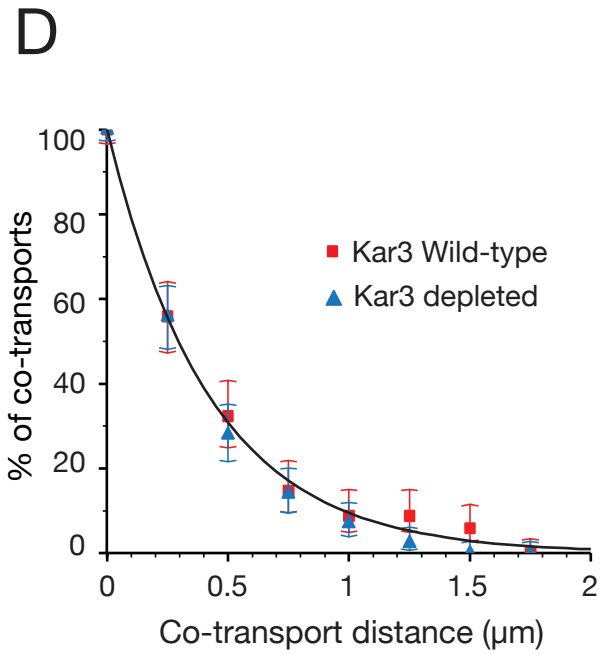

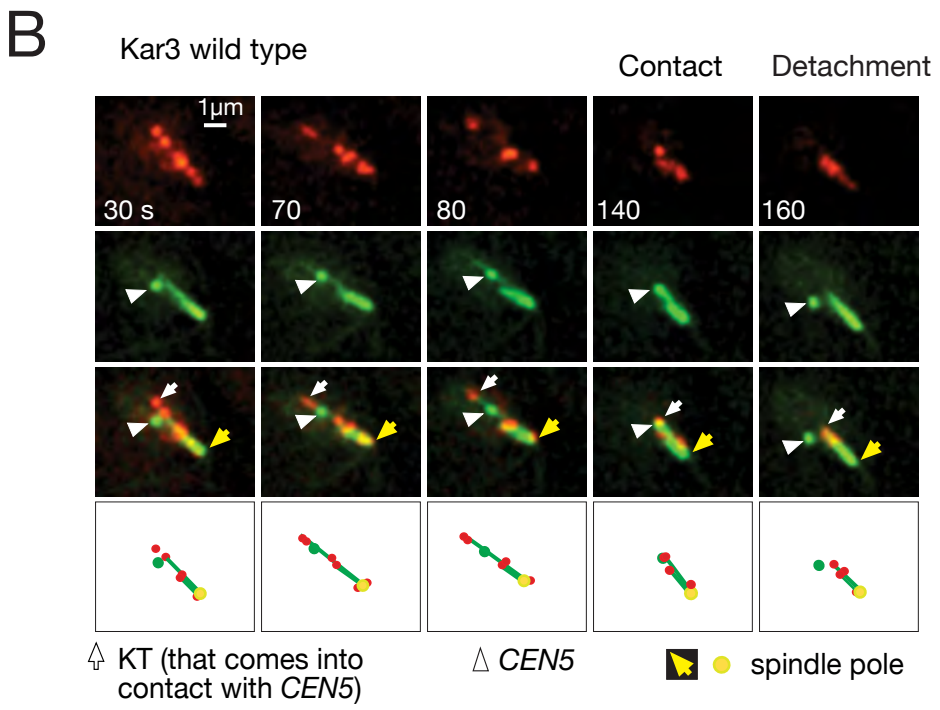

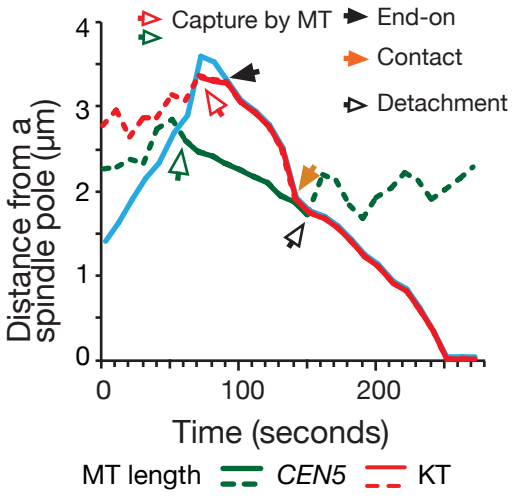

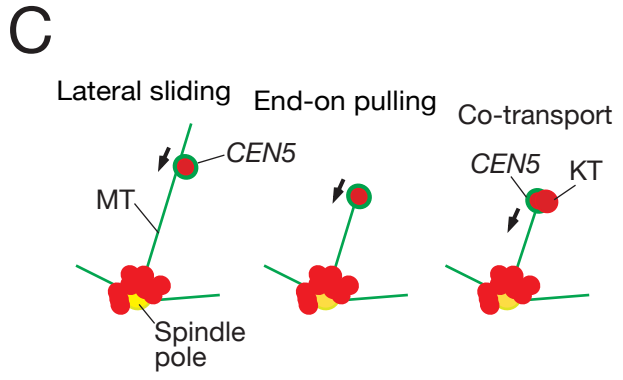

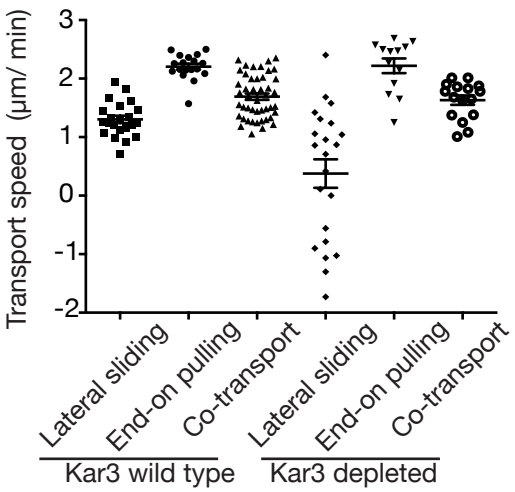

Figure S3. Supplemental Figure associated with Figure 4

A) The reason for visualizing one *CEN* and KTs to analyze KT detachments in physiological conditions. To analyze the outcome of two KTs interacting with a single MT (e.g. KT detachment), we initially visualized two *CEN*s in physiological conditions. In contrast to cells arrested in mitosis (see the legend for Figure S2A), two *CEN*s did not associate with each other before they interacted with MTs. However, two *CEN*s rarely interacted with the same MT. Second, we visualized KTs and, in some cases, one KT seemed to detach after a laterally-attached KT came into contact with a KT at the MT end (A, top). However, it was not easy to discern a KT detachment, because it was possible that newly formed KTs were interpreted incorrectly as detached KTs. To overcome this problem, we visualized one *CEN* and KTs, and analyzed the cases where the *CEN* and one KT (on another *CEN*) interacted with, presumably, a single MT (A, bottom; *CEN* closer to a spindle pole and the KT further from it). In this condition, we could clearly discern detachment of the *CEN*.

B) A representative example of *CEN5* detachment (following contact with an end-on attached KT [not on *CEN5*]) in a Kar3 wild-type cell with physiological condition. T11435 cells (see the legend for Figure 4C) were treated and images were acquired as in Figure 4A.

C) The speed of KT end-on pulling, sliding, and co-transport in physiological conditions. T11435 cells (see Figure 4C) were treated, and images were acquired, as in Figure 4C. The speed of *CEN5* motion in each mode was measured. To measure the co-transport speed, we chose samples where *CEN5* on the MT lateral side came into contact with a KT (on another *CEN*) at the end of, presumably, the same MT. Graphs show individual data points and mean ± SEM.

D) Detachment of *CEN* from the MT end occurs at a similar rate in Kar3 wild-type and Kar3-depleted cells, during co-transports of *CEN5* and a KT (at a different *CEN*) following their contact (refer to the diagram in Figure 4B), in physiological conditions. The images collected for Figure 4 were analyzed further. The graph shows how the percentage of co-transports of *CEN5* and a KT decreases as the co-transport proceeds and detachment of *CEN5* takes place. The measured percentage is shown for Kar3 wild-type (red squares) and Kar3-depleted (blue triangles) cells and the error bars represent standard errors of proportions. The percentage of remaining co-transports (in which detachment of *CEN5* has not occurred yet) declines similarly between Kar3 wild-type and Kar3-depleted cells, suggesting that the rate of *CEN5* detachment (per length of a co-transport) is similar between the two cells. The percentage also declines approximately following a simple exponential decay curve (black line), suggesting that detachment of one *CEN* happens approximately at a constant rate. Note that the rate of KT detachment is higher in physiological conditions (this figure) than in the centromere re-activation assay (Figure S2B). The reason for this difference is unclear. However, the number of molecules of KT components is higher with the centromere-reactivation assay, compared in physiological conditions, when KTs initially interact with MTs (Kitamura et al., 2007). A higher number of KT components (such as the Ndc80 complex) may allow a laterally attached KT to stay in the vicinity of the MT end (which is occupied by an end-on attached KT) for a longer period.

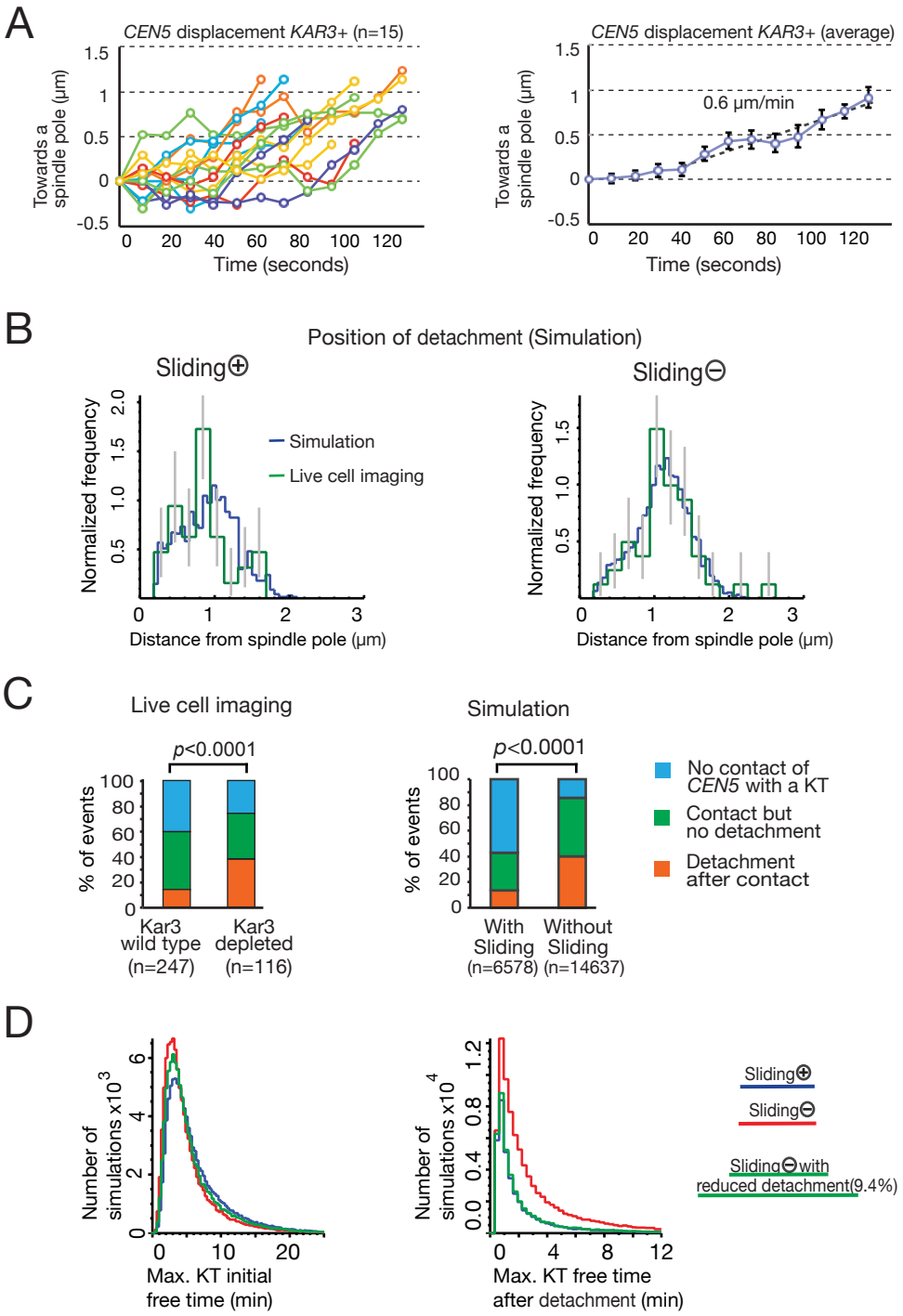
A
CEN5 displacement KAR3+ (n=15)
Towards a spindle pole (µm)
Time (seconds)
CEN5 displacement KAR3+ (average)
0.6 µm/min
B
Position of detachment (Simulation)
Sliding⊕
Sliding⊖
Simulation
Live cell imaging
Normalized frequency
Distance from spindle pole (µm)
C
Live cell imaging
Simulation
p<0.0001
% of events
Kar3 wild type (n=247)
Kar3 depleted (n=116)
With Sliding (n=6578)
Without Sliding (n=14637)
No contact of CEN5 with a KT
Contact but no detachment
Detachment after contact
D
Number of simulations x10^3
Max. KT initial free time (min)
Number of simulations x10^4
Max. KT free time after detachment (min)
Sliding⊕
Sliding⊖
Sliding⊖ with reduced detachment(9.4%)

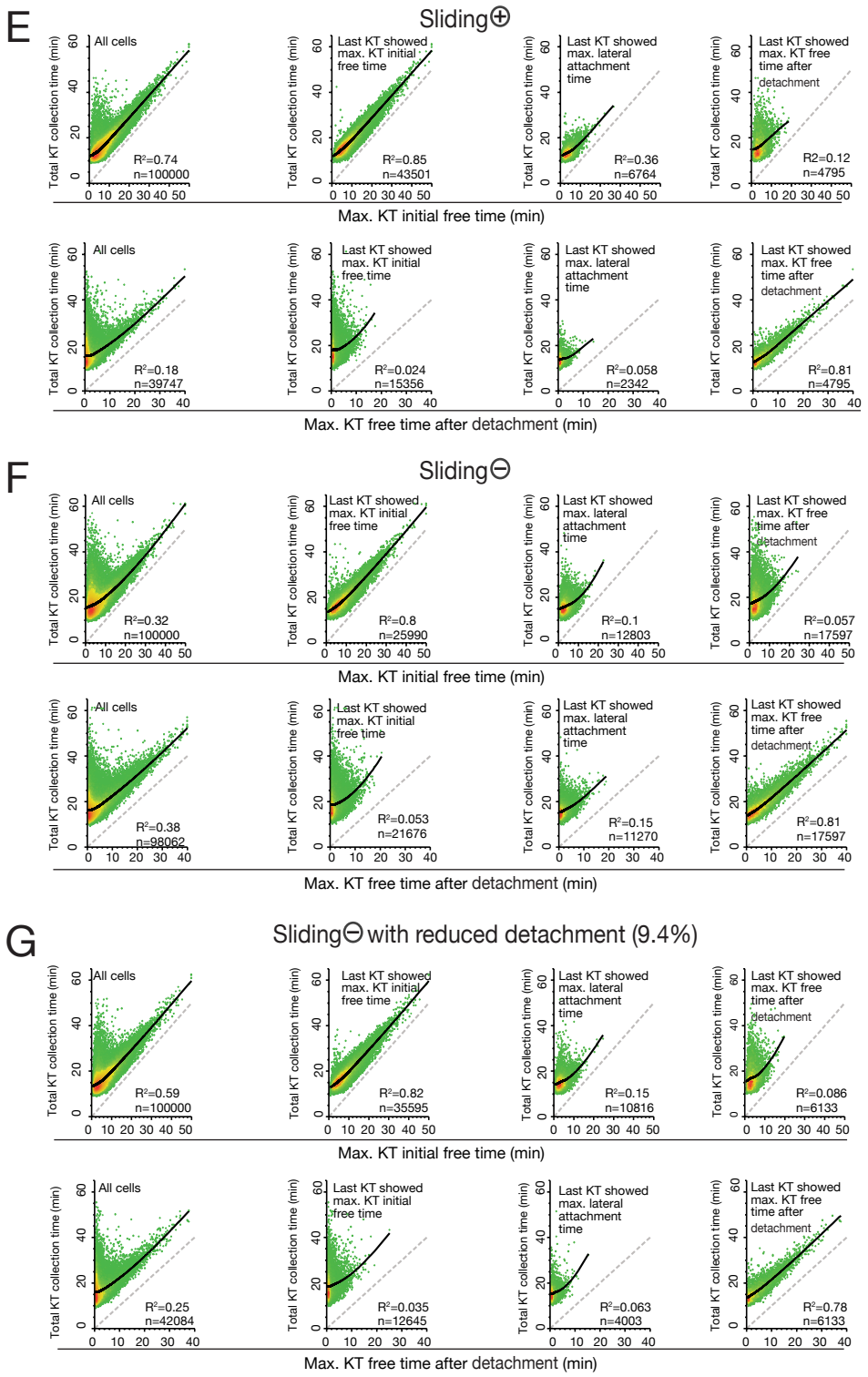
E
Sliding⊕
All cells
Last KT showed max. KT initial free time
Last KT showed max. lateral attachment time
Last KT showed max. KT free time after detachment
Total KT collection time (min)
R²=0.74 n=100000
R²=0.85 n=43501
R²=0.36 n=6764
R2=0.12 n=4795
Max. KT initial free time (min)
R²=0.18 n=39747
R²=0.024 n=15356
R²=0.058 n=2342
R²=0.81 n=4795
Max. KT free time after detachment (min)
F
Sliding⊖
R²=0.32 n=100000
R²=0.8 n=25990
R²=0.1 n=12803
R²=0.057 n=17597
R²=0.38 n=98062
R²=0.053 n=21676
R²=0.15 n=11270
R²=0.81 n=17597
G
Sliding⊖ with reduced detachment (9.4%)
R²=0.59 n=100000
R²=0.82 n=35595
R²=0.15 n=10816
R²=0.086 n=6133
R²=0.25 n=42084
R²=0.035 n=12645
R²=0.063 n=4003
R²=0.78 n=6133

Figure S4. Supplemental Figure associated with Figure 5

A) Quantifying the average speed of KT displacement along a MT. Cells (T7470) with *CEN5-tetOs TetR-3×CFP GFP-TUB1* was treated and images were acquired as in Figure 4A except that NAA was not added. Graph on left shows the position of *CEN5* for a short period, during which it was on the MT lateral side but not at the MT plus end. Each line represents a time course trajectory of *CEN5* along a MT in an individual cell. On x-axis and y-axis, zero represents the time and position (along a MT), respectively, of the initial *CEN5* capture by the MT lateral side. Plus values on y-axis represent *CEN5* displacement towards a spindle pole. Graph on right shows the displacement of *CEN5* from its original position along a MT, averaged among different cells shown in the left graph, while *CEN5* is on the MT lateral side. Error bars show standard errors of means. We interpret that *CEN5* motion is relatively slow during 0–40 seconds, compared with a later period. We reason that, in some cells, *CEN5* may not be physically on a MT during this period (note that an overlap of a *CEN5* signal with a MT signal does not necessarily mean physical *CEN5*-MT interaction because of limited spatial resolution in light microscopy). Thus we analyzed the average *CEN5* motion during 40–120 seconds, and estimated that the average speed of *CEN5* displacement was 0.6 μm/min towards a spindle pole along a MT. Note that the speed of KT lateral sliding in Figures S1C, S2A and S3C shows the speed when KT was moving continuously (see details in legends of Figures S1C, S2A and S3C). However a KT on the MT lateral side may also show short pausing and a brief motion away from a pole (see graph on left, this figure). Graph on right of this figure shows the average speed of KT displacement, including short pausing and brief motion away from a spindle pole. Therefore the average KT displacement speed measured in this figure is smaller than the average KT sliding speed in Figure S3C.

B) Positions of *CEN5* detachments distribute similarly in live-cell imaging and in simulation. Left graph shows *CEN5* detachment positions with KT sliding (*KAR3*+ wild-type in live-cell imaging), while right graph shows those without KT sliding (Kar3 depletion in live cell imaging). In both graphs, green line shows results from live cell imaging (Figure 4C, right) and blue line shows results from simulation. X-axis shows distance of *CEN5* detachments from a spindle pole (categorized in bins; 0.1875 and 0.06 μm interval for green and blue, respectively), while y axis- shows normalized frequency. Gray bars show standard errors of proportion in live-cell imaging results.

C) Frequency of *CEN5* detachments (orange) is similar in live-cell imaging (left) and in simulation (right). Graphs show how *CEN5* reaches a spindle pole or shows detachment, after *CEN5* and another KT are caught on the same MT. For live-cell imaging data, graphs in Figure 4D are copied here for comparison. Three categories are explained in Figure 4D legend (refer to Figure 4B). Frequency of the three categories was also obtained in 100,000 simulations with and without KT sliding. Note that the sample number (n number) is larger with Kar3 wild-type than with Kar3 depletion in live-cell imaging whereas it is larger without sliding than with sliding in simulation; this is because a larger number of Kar3 wild-type cells were observed in live-cell imaging in order to analyze a sufficient number of detachments with Kar3 wild-type.

D) Maximum KT initial free time and maximum KT free time after detachment. We have analyzed a maximum time (among 16 KTs) of KT being active but left unattached to a MT after moving away from a spindle pole following centromere replication (Max. KT initial free time; left) and a maximum time (among all detachment events in each simulation) of KT being left unattached to a MT following detachment after contact of two KTs on the same MT (Max. KT free time after detachment; right), in the three conditions analyzed in Figure 5C and D. The graphs show the numbers of simulations (y-axis) with these maximum times (x-axis), categorized in each bin (0.32 min interval).

E–G) The behavior of the last KT in individual simulations has been analyzed. How do

the diminished detachments, following contact of two KTs on the same MT, shorten the total KT collection time? In other words, how do more frequent KT detachments lead to a longer total KT collection time? To address this, we investigated the last KT that reached to the vicinity of a spindle pole (and formed end-on attachment to a short MT there), as it determines the total KT collection time in each simulation. More specifically, we addressed whether the last KT spent a long time in the following process: 1) being active but left unattached to a MT after moving away from a spindle pole following centromere replication (KT initial free time); 2) being left unattached to a MT following an detachment after contact of two KTs (KT free time after detachment); and/or 3) being on the MT lateral side (lateral attachment time). We compared the amount of time spent by each KT in 1), 2) and 3) among all KTs or among all relevant events in each simulation, and identified the KT that spent the longest time in each process. Then individual simulations were categorized into three subgroups, in which the last KT was identical to the KT that spent the longest time in 1), 2) and 3); i.e. the last KT showed 'max. KT initial free time', 'max. KT free time after detachment' and 'max. lateral attachment time' (if a simulation belonged to two or three subgroups, it was not included in further analyses). In each subgroup, we plotted total KT collection time against 'max KT initial free time' and 'max KT free time after detachment' in individual simulations (if no KT showed detachment in a simulation, that simulation was not included in plotting against 'max KT free time after detachment'). This analysis was carried out with the three conditions analyzed in Figure 5C and D, and the results are shown in A, B and C. In each graph, red and green represents high and low density of samples, respectively; a dashed line shows the line x=y; a black line represents a loess curve, which shows locally weighted polynomial regression that smooths y values against a local change along x-axis; a R squared is a coefficient of determination showing how well data points follow the loess curve. We interpret that, when total KT collection time showed high correlation with 'max. KT initial free time' or 'max. KT free time after detachment', the total KT collection time was determined by such maximum time. When KT sliding was present (A), the majority of the last KT showed 'max. KT initial free time', determining total KT collection time. When KT sliding was switched off (B), there was a substantial increase in the population (from 4795 to 17597), in which the last KT experienced 'max. KT free time after detachment', determining total KT collection time (B, bottom right). When detachment frequency was reduced to 9.4 % in the absence of KT sliding (C), this population was reduced to a level (6133) close to that with KT sliding (4795). Overall these results suggest that, after frequent KT detachments (following contact of two KTs) in the absence of KT sliding, some detached KTs spent a long time before being recaptured by a MT and became the last KT reaching a spindle pole, which prolonged total KT collection time.

Table S1. Yeast strains used in this study

The table shows genotypes of yeast strains used in this study. All strains used in this study are derivatives of *Saccharomyces cerevisiae* W303 (K699 and K700 from Kim Nasmyth lab).

Strain	Genotype
T6519	*MATalpha P_{GAL}-CEN3-lacOs::URA3 his3::GFP-lacI::HIS3 cen15Δ::P_{GAL}-CEN3-tetOs::URA3 ade1::TetR-3xCFP::hphMX trp1::P_{TUB1}YFP-TUB1::TRP1 P_{MET3}-CDC20::TRP1*
T7470	*MATa CEN5::tetOs::HIS3 leu2::tetR-3xECFP::HPH1 ura3::P_{TUB1}-GFP-TUB1::URA3*
T9717	*MATa P_{GAL}-CEN3-lacOs::URA3 his3::GFP-lacI::HIS3 cen15Δ::P_{GAL}-CEN3-tetOs::URA3 ade1::TetR-3xCFP::hphMX trp1::GFP-TUB1::TRP1 P_{MET3}-CDC20::TRP1*
T10013	*MATa kar3Δ::kanMX P_{GAL}-CEN3-lacOs::URA3 his3::GFP-lacI::HIS3 cen15Δ::P_{GAL}-CEN3-tetOs::URA3 ade1::TetR-3xCFP::hphMX trp1::GFP-TUB1::TRP1 P_{MET3}-CDC20::TRP1*
T10546	*MATa cen15Δ::P_{GAL}-CEN3-tetOs::URA3 ade1::TetR-3xCFP::hphMX his3::GFP-TUB1::HIS3 RPL13A-2xFKBP12::TRP1 TOR1-1 fpr1Δ::natMX4 P_{MET3}-CDC20::TRP1*
T11434	*MATa KAR3-aid::natNT2 ura3::P_{ADH1}-TIR1::URA3 MTW1-4xmCherry::natMX6 CEN5::tetOs::HIS3 leu2::tetR-GFP::LEU2 Ndc80-4mCherry::NatMX6 his3::P_{TUB1}-GFP-TUB1::HIS3*
T11435	*MATalpha ura3::P_{ADH1}-TIR1::URA3 MTW1-4xmCherry::natMX6 Ndc80-4mCherry::natMX6 CEN5::tetOs::HIS3 leu2::tetR-GFP::LEU2 his3::P_{TUB1}-GFP-TUB1::HIS3*
T11469	*MATa KAR3-aid::natNT2 SLK19-aid::kanMX ura3::P_{ADH1}-TIR1::URA3 P_{GAL}-CEN3-lacOs::URA3 his3::GFP-lacI::HIS3 cen15Δ::P_{GAL}-CEN3-tetOs::URA3 ade1::TetR-3xCFP::hphMX trp1::GFP-TUB1::TRP1 P_{MET3}-CDC20::TRP1*
T11497	*MATa SLK19-aid::kanMX ura3::P_{ADH1}-TIR1::URA3 P_{GAL}-CEN3-lacOs::URA3 his3::GFP-lacI::HIS3 cen15Δ::P_{GAL}-CEN3-tetOs::URA3 ade1::TetR-3xCFP::hphMX trp1::GFP-TUB1::TRP1 P_{MET3}-CDC20::TRP1*
T11941	*MATa cen15Δ::P_{GAL}-CEN3-tetOs::URA3 ade1::TetR-3xCFP::hphMX his3::GFP-TUB1::HIS3 leu2::GFP-TUB1::LEU2 SCC1-FRB::kanMX6 RPL13A-2xFKBP12::TRP1 TOR1-1 fpr1Δ::natMX4 P_{MET3}-CDC20::TRP1*

Table S2. Parameters and their values used in simulation

The table shows parameters and their values used in the computer simulation shown in Figures 5 and S4.

Parameter	Symbol	Value	Source of the value
Time step	Δt	0.001 min	A reasonably small value was chosen
Radius of the nucleus	R_{nuc}	1.25 μm	Natsume et al, 2013 (visualization of the nuclear envelope)
Initial MT number	n_{MT}	5	Based on Fig S1E etc. Kitamura et al., 2010
Exclusion radius	r_{ex}	0.2 μm	Based on Fig S1E etc. Kitamura et al., 2010
MT growth speed	v_{gro}	1.5 μm min^{-1}	Fig 3b, Tanaka et al. 2005
MT shrinkage speed	v_{shr}	2.8 μm min^{-1}	Fig 3b, Tanaka et al. 2005
MT catastrophe rate	K_{cat}	0.6 min^{-1}	Gandhi et al, 2011
MT nucleation rate	K_{nuc}	1 min^{-1}	Based on Fig S1E etc. Kitamura et al., 2010
MT beaming factor	β	0.7	Based on Fig S1E etc. Kitamura et al., 2010
MT angular diffusion coefficient	D_{MT}	0.03 rad^2 min^{-1}	Based on Kalinina et al 2013
Diffusion coefficient	D	0.1 μm^2 min^{-1}	Fig S1, Kitamura et al., 2007
KT activation delay	t_{del}	2 min	Gandhi et al, 2011
KT lateral displacement speed	v_{lat}	0.6 μm min^{-1}	This study
KT lateral diffusion coefficient	D_{lat}	0.1 μm^2 min^{-1}	Fig 3, Tanaka et al. 2007
KT detachment rate	K_{evi}	4.8 μm^{-1}	This study
KT end-on pulling speed	v_{pul}	1.7 μm min^{-1}	Fig 2D, Tanaka et al. 2007 & Fig 7C, Kitamura et al. 2007
KT slow end-on pulling speed	v_{spul}	0.35 μm min^{-1}	Gandhi et al., 2011
KT co-transport speed	v_{tran}	1.4 μm min^{-1}	This study
KT rescue delay	t_d	8 sec	Gandhi et al., 2011
Stu2 sending rate	K_{stu2}	0.1 min^{-1}	Gandhi et al., 2011
Stu2 speed	v_{stu2}	2.1 μm min^{-1}	Fig S9, Tanaka et al. 2005 & Gandhi et al., 2011
KT capture radius	R_{KT}	0.4 μm	Fig 6A, S6A Kitamura et al., 2010
KT capture speed	v_{cap}	5 μm min^{-1}	Fig S1C, Kitamura et al., 2010
Probability of MT rescue at the KT	P_{res}	0.6	Fig 4B, Tanaka et al., 2007

Supplemental Movies

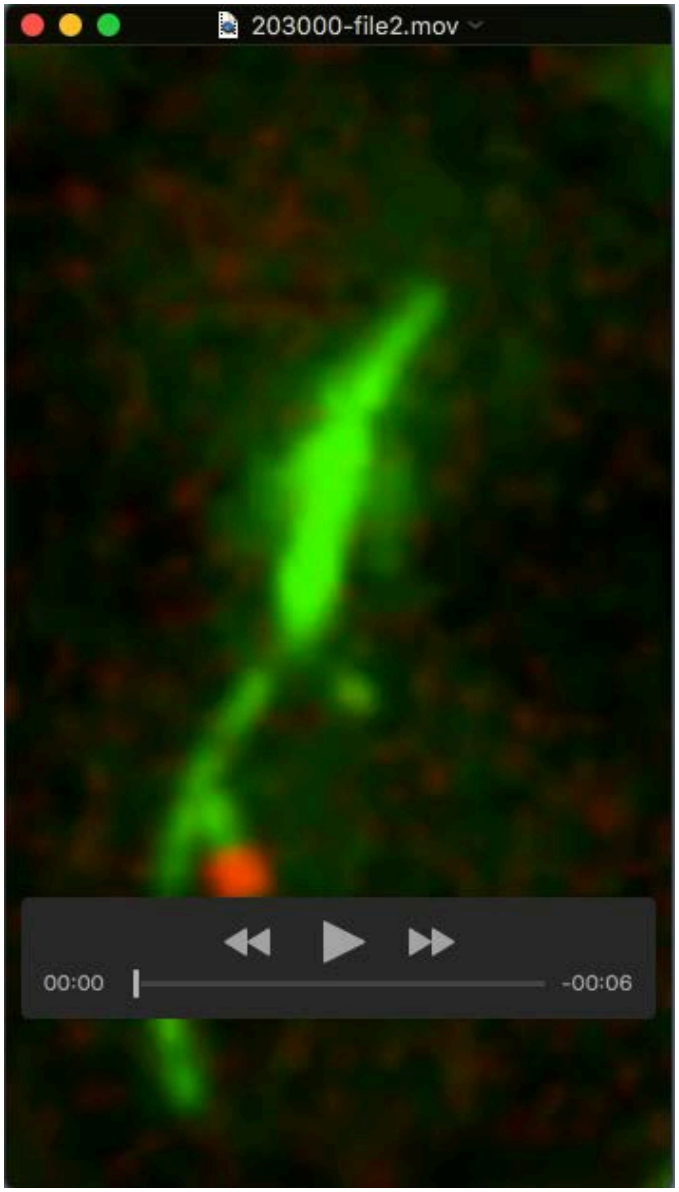

Movie 1. A representative example is shown in which two *CEN*s (two pairs of sister *CEN*s) showed lateral sliding along a single MT (associated with Figure 1C). The procedure of the experiment is explained in the legend for Figure 1C. Green shows the spindle, MTs and *CEN* on chromosome *III* while red shows *CEN* on chromosome *XV*. The interval of frames is 20 sec, and 5 frames are shown per second in the movie.

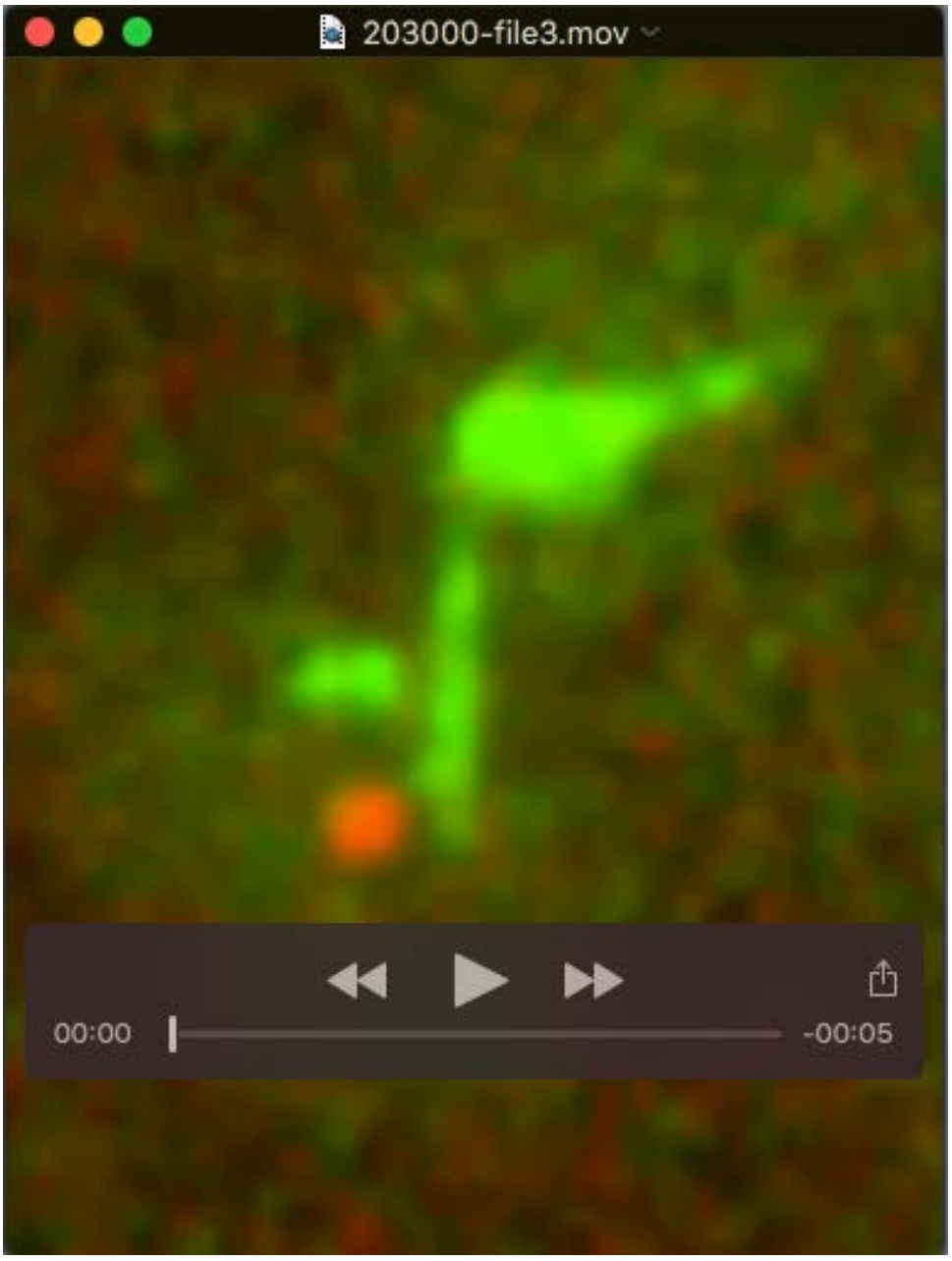

Movie 2. A representative example is shown in which a laterally attached *CEN* showed detachment after coming into contact with an end-on attached *CEN* (associated with Figure 1D). The procedure of the experiment is explained in the legend for Figure 1D. Green shows the spindle, MTs and *CEN* on chromosome *III* while red shows *CEN* on chromosome *XV*. The interval of frames is 13 sec, and 5 frames are shown per second in the movie.

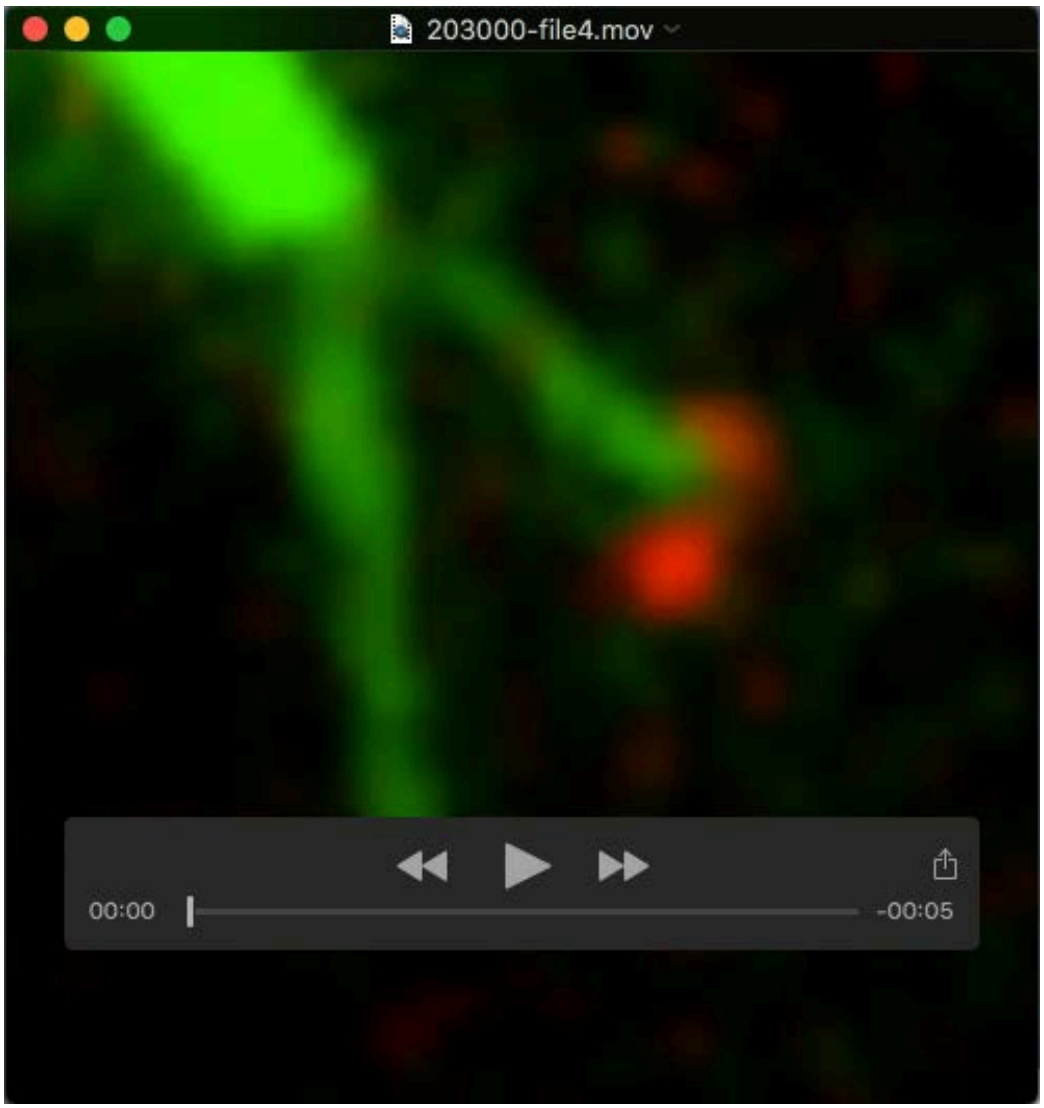

Movie 3. A representative example is shown in which sister *CEN*s interact with a single MT after their cohesion is lost (associated with Figure 2B). The procedure of the experiment is explained in the legend for Figure 2B. Green shows the spindle and MTs while red shows *CEN* on chromosome *XV*. The interval of frames is 10 sec, and 5 frames are shown per second in the movie.

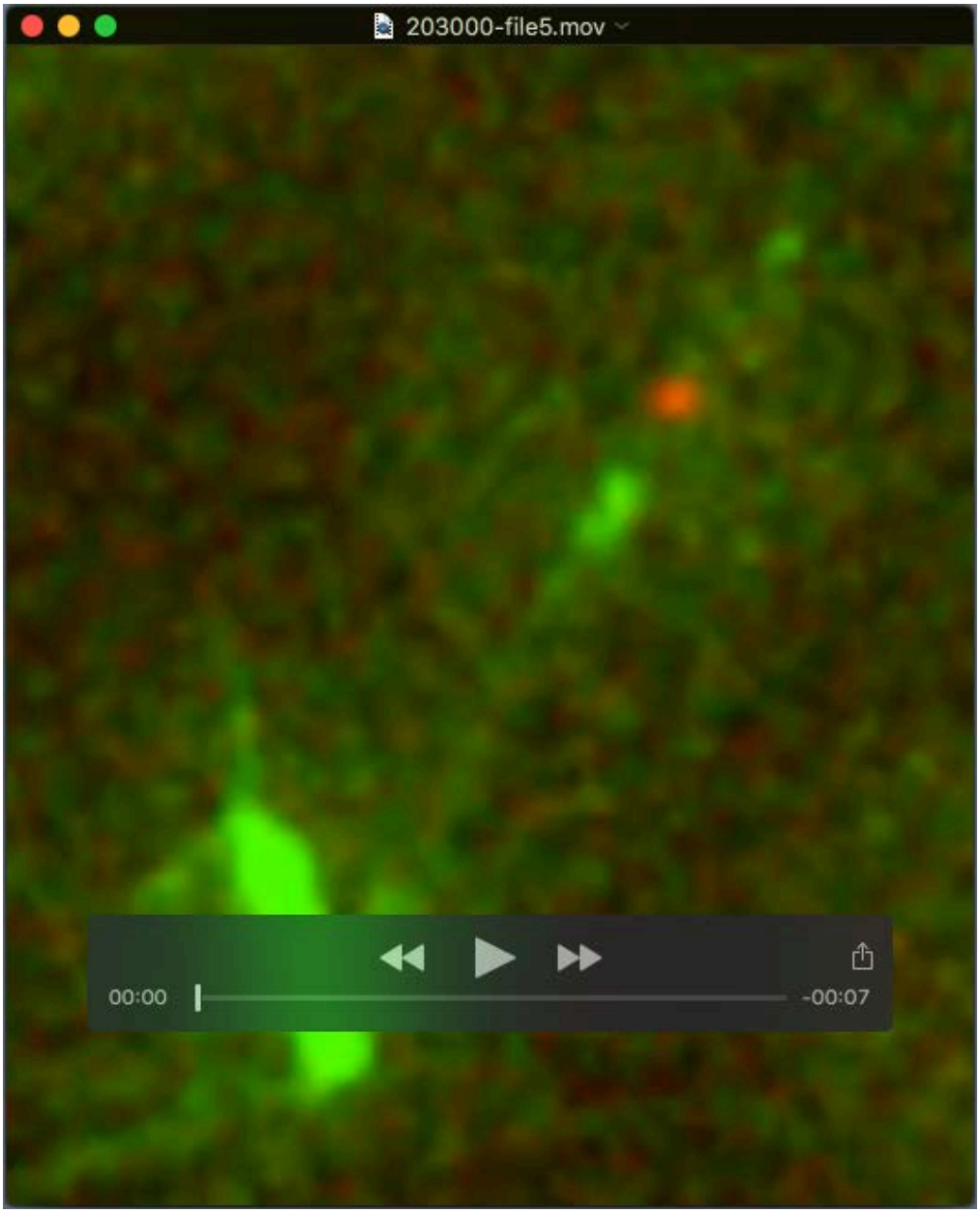

Movie 4. A representative example of a Kar3-depleted cell in which a laterally attached *CEN* showed detachment after coming into contact with an end-on attached *CEN* (associated with Figure 3A). The procedure of the experiment is explained in the legend for Figure 3A. Green shows the spindle, MTs and *CEN* on chromosome *III* while red shows *CEN* on chromosome *XV*. The interval of frames is 18 sec, and 5 frames are shown per second in the movie.

Journal of Cell Science • Supplementary information

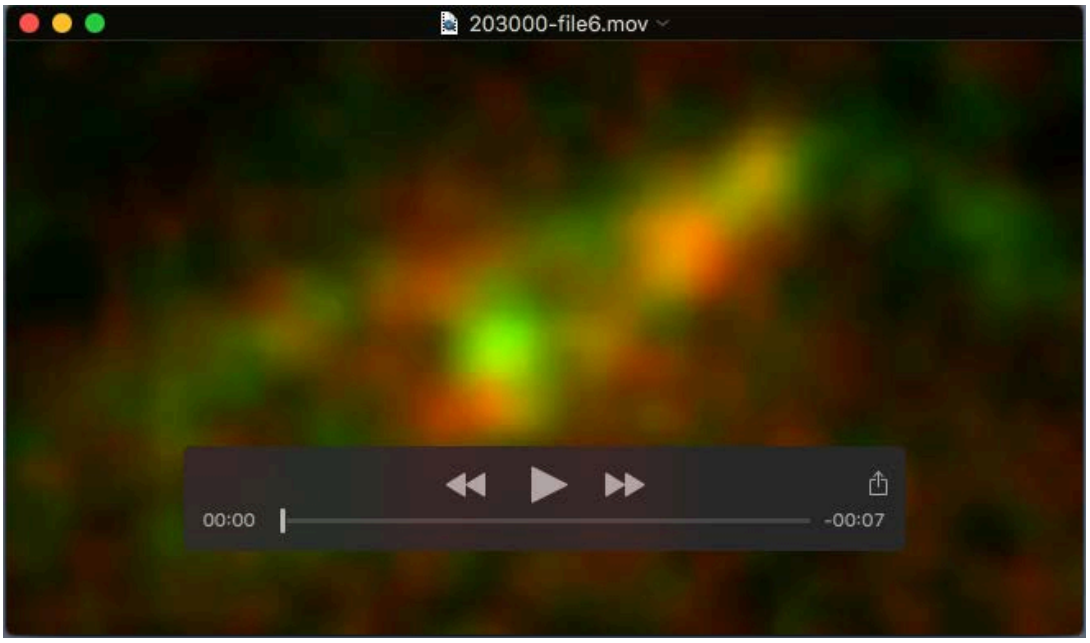

Movie 5. A representative example of *CEN* detachment is shown in physiological condition (associated with Figure 4A). The procedure of the experiment is explained in the legend for Figure 4A. Green shows the spindle, MTs and *CEN5* while red shows KTs. The interval of frames is 10 sec, and 5 frames are shown per second in the movie. Note that, after showing detachment at 210 s, *CEN5* was out of focus during 230-310 s, during which *CEN5* distance from a spindle pole was measured using out-of-focus *CEN5* signals.

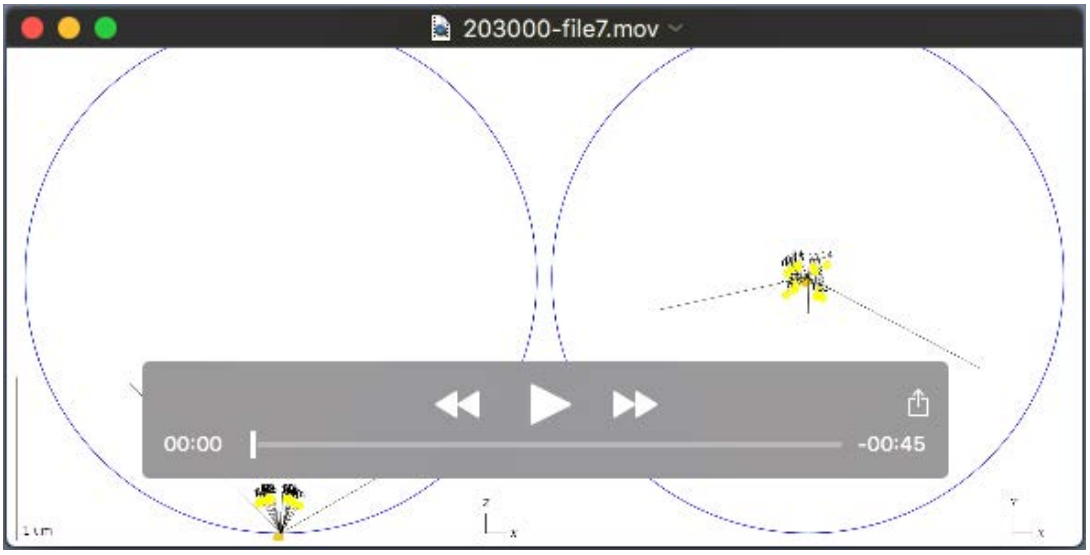

Movie 6. A representative example of computer simulation is shown with KT sliding (normal condition, i.e. with KT sliding; associated with Figure 5). Three-dimensional simulations are projected into X-Z and X-Y planes. KTs (dots) are colored as in Figure 5A. MT extension following KT-dependent rescue is shown in a dashed line (Gandhi et al., 2011). A gray line, which connects a KT (dot) to a MT extending from a spindle pole (black line), represents a KT-derived MT that facilitates KT loading onto a MT extending from a spindle pole (Kitamura et al., 2010).

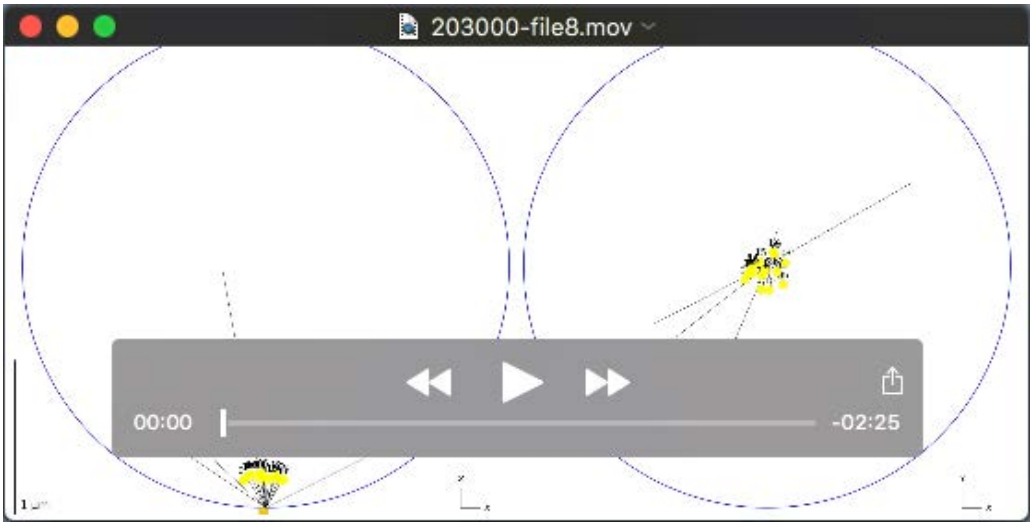

Movie 7. A representative example of computer simulation is shown without KT sliding (associated with Figure 5B). Three-dimensional simulations are projected into X-Z and X-Y planes. KTs (dots) are colored as in Figure 5A. MT extension following KT-dependent rescue is shown in a dashed line (Gandhi et al., 2011). A gray line, which connects a KT (dot) to a MT extending from a spindle pole (black line), represents a KT-derived MT that facilitates KT loading onto a MT extending from a spindle pole (Kitamura et al., 2010).

Supplemental References

Brun, L. (2011). Search and capture model in different DNA segregation processes. In *Physics*, vol. PhD, pp. 64-88: EMBL, Heidelberg.

Gandhi, S. R., Gierlinski, M., Mino, A., Tanaka, K., Kitamura, E., Clayton, L. and Tanaka, T. U. (2011). Kinetochore-dependent microtubule rescue ensures their efficient and sustained interaction in early mitosis. . *Dev Cell* **21**, 920-933.

Gonen, S., Akiyoshi, B., Iadanza, M. G., Shi, D., Duggan, N., Biggins, S. and Gonen, T. (2012). The structure of purified kinetochores reveals multiple microtubule-attachment sites. *Nat Struct Mol Biol* **19**, 925-9.

Kalantzaki, M., Kitamura, E., Zhang, T., Mino, A., Novak, B. and Tanaka, T. U. (2015). Kinetochore-microtubule error correction is driven by differentially regulated interaction modes. *Nat Cell Biol.* **17**, 421-33.

Kalinina, I., Nandi, A., Delivani, P., Chacon, M. R., Klemm, A. H., Ramunno-Johnson, D., Krull, A., Lindner, B., Pavin, N. and Tolic-Norrelykke, I. M. (2013). Pivoting of microtubules around the spindle pole accelerates kinetochore capture. *Nat Cell Biol* **15**, 82-7.

Kitamura, E., Tanaka, K., Kitamura, Y. and Tanaka, T. U. (2007). Kinetochore microtubule interaction during S phase in Saccharomyces cerevisiae. *Genes Dev* **21**, 3319-30.

Kitamura, E., Tanaka, K., Komoto, S., Kitamura, Y., Antony, C. and Tanaka, T. U. (2010). Kinetochores generate microtubules with distal plus ends: their roles and limited lifetime in mitosis. *Dev Cell* **18**, 248-59.

Lampert, F., Hornung, P. and Westermann, S. (2010). The Dam1 complex confers microtubule plus end-tracking activity to the Ndc80 kinetochore complex. *J Cell Biol* **189**, 641-9.

Maure, J. F., Komoto, S., Oku, Y., Mino, A., Pasqualato, S., Natsume, K., Clayton, L., Musacchio, A. and Tanaka, T. U. (2011). The Ndc80 loop region facilitates formation of kinetochore attachment to the dynamic microtubule plus end. *Curr Biol* **21**, 207-13.

Natsume, T., Muller, C. A., Katou, Y., Retkute, R., Gierlinski, M., Araki, H., Blow, J. J., Shirahige, K., Nieduszynski, C. A. and Tanaka, T. U. (2013). Kinetochores coordinate pericentromeric cohesion and early DNA replication by cdc7-dbf4 kinase recruitment. *Mol Cell.* **50**, 661-74.

Richmond, D., Rizkallah, R., Liang, F., Hurt, M. M. and Wang, Y. (2013). Slk19 clusters kinetochores and facilitates chromosome bipolar attachment. *Mol Biol Cell.* **24**, 566-77.

Tanaka, K., Kitamura, E., Kitamura, Y. and Tanaka, T. U. (2007). Molecular mechanisms of microtubule-dependent kinetochore transport toward spindle poles. *J Cell Biol* **178**, 269-81.

Tanaka, K., Mukae, N., Dewar, H., van Breugel, M., James, E. K., Prescott, A. R., Antony, C. and Tanaka, T. U. (2005). Molecular mechanisms of kinetochore capture by spindle microtubules. *Nature* **434**, 987-94.

Tien, J. F., Umbreit, N. T., Gestaut, D. R., Franck, A. D., Cooper, J., Wordeman, L., Gonen, T., Asbury, C. L. and Davis, T. N. (2010). Cooperation of the Dam1 and Ndc80 kinetochore complexes enhances microtubule coupling and is regulated by aurora B. *J Cell Biol* **189**, 713-23.